Journal of Peptide Science
J. Pept. Sci. 2008; **14**: 461–468
Published online 13 November 2007 in Wiley InterScience (www.interscience.wiley.com). DOI: 10.1002/psc.948

JOURNAL OF PEPTIDE SCIENCE

X-ray reflectivity study of a transcription-activating factor-derived peptide penetration into the model phospholipid monolayers‡

GIYOONG TAE,[a] HOSUNG YANG,[a] KWANWOO SHIN,[b]* SUSHIL K. SATIJA[c] and NAOYA TORIKAI[d]

[a] Department of Materials Science and Engineering, GIST, Gwangju, Korea
[b] Department of Chemistry and Program of Integrated Biotechnology, Sogang University, Seoul, Korea
[c] NIST Center for Neutron Research, Gaithersburg, MD, USA
[d] High Energy Accelerator Research Organization, Tsukuba, Ibayaki, Japan

Received 28 June 2007; Revised 14 August 2007; Accepted 31 August 2007

Abstract: The penetration of a transcription-activating factor (TAT)-derived, cell-penetration peptide onto 1,2-dipalmitoyl-*sn*-glycero-3-phosphocholine (DPPC) or 1,2-dipalmitoyl-*sn*-glycero-3-[phospho-L-serine] (DPPS) monolayer on phosphate-buffered saline subphase was characterized. The surface area at the target pressure increased noticeably by the peptide penetration from the subphase to the phospholipid monolayer, which might suggest a direct penetration of the peptide across the pure phospholipid bilayer membrane. Interestingly, the more significant area increase at 35 mN/m was monitored from DPPC monolayer, contrary to the simple charge interaction: the net neutral DPPC, the net-negative DPPS, and the positive TAT-derived peptides (TDP). X-ray reflectivity measurements as well as the molecular area from π (surface pressure)-*A* (area) isotherms suggest that the packing density of DPPS at the target pressure is too high to allow the effective penetration of the peptide into the monolayer and the positively charged peptides can be entrapped at the negative electrostatic well of DPPS headgroup layer, leading to the simple adsorption on the DPPS monolayer instead of penetration into it. Thus, more penetration with less adsorption of the peptide is induced by DPPC monolayer than DPPS monolayer. Copyright © 2007 European Peptide Society and John Wiley & Sons, Ltd.

Keywords: cell-penetrating peptide; DPPC; DPPS; X-ray reflectivity; Langmuir; BAM

INTRODUCTION

Cell-penetrating peptides (CPPs) or protein-transduction domains (PTDs) are the short peptides that can traverse cell membranes efficiently, thus translocate the attached cargo into the cytosol of the cells. They are short in size (less than 30 amino acids), and typically have strong net positive charge [1]. Their translocation efficiency is so high and universal that they can cargo into most of the cell types, from small peptides to even massive particles up to 200 nm in size. CPPs are also effective regardless of the attachment method with cargo (conjugated, complexed, or fused) [2] or the attachment position (*N*-terminus, *C*-terminus, or center) [3]. Therefore, the attachment of CPPs can be a versatile tool for intracellular drug delivery systems, especially for biological drugs such as peptides, proteins, or genes. In addition, CPPs have many potential *in vitro* applications such as drug discovery and laboratory assays that utilize the intracellular delivery of biomolecules and macromolecular cargo [2].

Reported CPPs so far are either the segments of existing proteins (protein-based) or synthetic (fusion or model amphiphatic). Protein-based CPPs include homeodomain-derived peptides, transcription-activating factor (TAT)-derived peptides (TDPs), and signal-sequence-based peptides [4]. Among them, TDP, having 11 key amino acid residues with mostly lysines and arginines (YGRKKRRQRRR), from the human immunodeficiency virus (HIV-1) TAT protein is the historic and most widely studied CPP [5,6]. TDP acts not only as a membrane traversing agent, but also as a nucleus localization agent [7].

Even though many results on the basic research about the cellular uptake of CPP-carrying cargos have been reported, the molecular mechanism of cell membrane translocation is still controversial and unclear. The essential characteristics of the cell membrane translocation by CPP, that are generally accepted, are energy-independent and nonreceptor mediated [7,8], despite some energy-dependent behavior also has been reported, specifically for TDP [3]. Considering highly net positive charges of CPPs, it is surprising that CPPs can traverse cell membranes efficiently without the use of receptors, especially maintaining the translocation efficiency when attached with large, hydrophilic macromolecules [9].

Most of the studies on CPPs are cell-based *in vitro* or *in vivo* experiments, thus the experiments with simple model system composed of lipids only are rather rare; the adsorption of TAT-derived peptides onto

* Correspondence to: Kwanwoo Shin, Department of Chemistry, Sogang University, Shinsoo, Mapo-gu, Seoul 121-742, Korea;
e-mail: kwshin@sogang.ac.kr
‡ This article is part of the Special Issue of the Journal of Peptide Science entitled "2nd workshop on biophysics of membrane-active peptides".

the model lipid monolayer composed of 1-palmitoyl-2-oleoyl-*sn*-glycero-3-phospho-*rac*-glycerol (POPG) and 1-palmitoyl-2-oleoyl-*sn*-glycero-3-phosphocholine (POPC) was characterized [9], and no insertion of the peptides into the lipid monolayer was observed at the packed state π (surface pressure) >30 mN/m. Thus, they concluded that the direct penetration of CPPs into lipid membrane is not possible. Therefore, first, the binding of the cationic CPP with negatively-charged, cell surface proteoglycans, such as heparan sulfate, to form an electrically neutral complex, followed by consecutive adsorptive endocytosis [10] was proposed as a cell membrane penetration mechanism by TDPs [9].

Here, we present the evidence of direct penetration of TDP into model lipid monolayers even at densely packed state (35 mN/m). Instead of POPG and POPC, we used 1,2-dipalmitoyl-*sn*-glycero-3-phosphocholine (DPPC), as a representative of the most abundant zwitterionic phospholipids, phophatidylcholines (PC) in human cell membrane, and 1,2-dipalmitoyl-*sn*-glycero-3-[phospho-L-serine] (DPPS) as a representative of net negatively-charged phospholipids, phosphatidylserines (PS) [11]. We measured the adsorption dynamics of TDP into the model lipid monolayer by monitoring the area change at constant surface pressure, and the domain morphology was characterized by various methods including *in situ* X-ray reflectivity. Since the reflected X-ray at the interfaces is highly sensitive to the electron density variation [12,13], X-ray reflectivity shows enough resolution to determine the changes of the lipid monolayer within a few angstroms. We found the direct penetration of TDP into the pure phospholipid monolayer. More interestingly, the more adsorption and penetration was observed into zwitterionic, net neutral DPPC monolayer than net negatively-charged DPPS monolayer. Our results suggest that there might exist a direct penetration pathway of the TDP cargo system via the cell membrane alone (phospholipid bilayer) without the assistance of other cell surface proteoglycan, in addition to other possible pathways.

MATERIALS AND METHODS

A synthesized TDP, H_3N^+-YGRKKRRQRRR-COO^-, with purity over 97%, was purchased from Anygen (Gwangju, Korea). DPPC and DPPS were purchased from Avanti Polar Lipids and used without further purification. For a subphase, phosphate-buffered saline (PBS) was prepared by mixing of 8 g of NaCl, 2 g of KCl, 1.44 g Na_2HPO_4, and 0.24 g of KH_2PO_4 in 1 l of deionized water, and then adjusted pH to 7.4 with concentrated HCl under constant mixing.

Surface pressure (π)–area (A) isotherms were recorded at a compression rate of 0.75 cm^2/min using a KSV Langmuir minitrough containing a PBS (pH = 7.4) subphase. The total compression area of the Langmuir trough was 300 cm^2, and it was placed in a Plexiglass enclosure. The temperature was maintained at room temperature (~25 °C) using an external water chiller. DPPC and DPPS powders were dissolved in chloroform and chloroform/methanol solution (4 : 1, v/v), respectively at a concentration of 0.5 mg/ml, and the phospholipid solutions were then spread onto the PBS subphase. The monolayers were then compressed to a target pressure of 35 mN/m, and maintained the target pressure by controlling the barrier position. A peristaltic pump, with inlet and outlet tubes placed at each end of the trough, was used to mix the subphase following the addition of TDP for 2 h at a rate of 4 ml/min. In order to ensure the cleanness of tubes and sensitivity of the system, a control experiment without the addition of TDP was performed, and no adsorption was observed. Upon the addition of concentrated TDP solution into the subphase, the TDP concentration in the subphase was controlled to be 5 μM. Prior to the subsequent reflectivity measurements, the *adsorption dynamics* on different phospholipid monolayers with respect to time was determined by constantly observing the changes in surface pressure. The stability of the entire system was ensured by placing the Langmuir trough on an active anti-vibration table.

A commercial Brewster angle microscope (BAM2plus, NFT, Germany) was used and mounted above a Langmuir trough to image the domain morphology of monolayers as a function of area per molecule. The *p*-polarized light from a 50-mW laser with a wavelength of 532 nm was reflected off the air/water interface with an angle of incidence close to the Brewster angle (53.1°) of subphase, which is given by the Snell's law of refraction, $tan(\theta) = n_{water}/n_{air}$, where n_i is the refractive index of a media i. The morphology of the monolayer was recorded by a CCD camera at different stages of the phase transitions. A zooming microscope with a 10× objective lens was used and the lateral resolution was 2 μm.

X-ray reflectivity was performed using a D8 Advance (Bruker Axs, Germany) with a vertical goniometer, which allows the study of a liquid surface, without disturbing a Langmuir trough during measurements. A ceramic anode X-ray generator was used to produce Cu K_α radiation (λ = 1.542 Å), followed by paralleling the incident beam with a Göbel mirror (GM III). Two slits prior to the sample defined the incident beam size and reduced the vertical divergence.

For the specular reflection, the scattering vector, $\boldsymbol{q} = \boldsymbol{k}_f - \boldsymbol{k}_i$, is only in the z-direction which is normal to the interface. Since $q_x = q_y = 0$, it is given by $q_z = (4\pi/\lambda)\sin\alpha_i$, where α_i is the incident angle. By the Born approximation at $q_z > 3q_c$, where q_c is the critical angle for total reflection, the reflectivity, $R(q_z)$, is expressed essentially:

$$R(q_z) \propto R_F \left| \int \frac{d\rho(z)}{dz} \exp(-iq_z z) \right|^2 \quad (1)$$

where R_F is the Fresnel reflectivity at an infinitely sharp interface and $\rho(z)$ is the electron density variation in perpendicular to a sample surface. Thus, by reflectivity measurement, it is possible to detect even a very small variation of adsorbed peptides which induce the density gradient to the z-direction. We repeatedly scanned the reflectivity to monitor the thickness (d) and the density changes of TDPs adsorbed on the phospholipids/liquid interface as a function of time. The dispersion, δ, which is a real part of the index of refraction, is given linearly in terms of the electron density, ρ, by $\delta = \lambda^2 \rho r_0/2\pi$, where r_0

DOI: 10.1002/psc

is the classical electron radius (2.82×10^{-13} cm). Therefore, dispersion profiles obtained from the reflectivity fits are essentially the same as the corresponding electron density profile [12]. Note that the electron density profiles shown in this paper, were converted from the dispersion profile obtained from the reflectivity fits.

To analyze the reflectivity data, the recursive Parratt formalism was used. The sharp interfaces are smeared by rms roughness, σ, which is given by convoluting the infinitely sharp profile with a Gaussian smoothing function. We systematically varied and then optimized the fitting parameters (ρ, d, and σ) until the sum of the squares of the offsets (χ^2) of the points from the curve was minimized.

RESULTS AND DISCUSSION

Monolayers of Model Phospholipids

The phospholipids used to make the model membrane are DPPC and DPPS, whose structures have palmitates (saturated hydrocarbon, carbon number, C = 16) as two fatty acid tail parts. DPPC has a positively charged choline as an alcohol part, whereas DPPS has an L-serine as an alcohol part. Thus, in conjunction with the negatively charged phosphate linkage in phospholipid structure, DPPC has no net charge, whereas DPPS has net-negative charge. As mentioned in the introduction part, both the phospholipids are used as representatives of the abundant phospholipid in human cells [11].

π-A isotherms of two model phospholipids are shown in Figure 1, when we spread them at the air/PBS interface. DPPC exhibits two transition states, typical characteristic of fatty acid monolayer. At about 5 mN/m, it shows the first transition from a liquid-expanded (LE) state to a liquid-compressed (LC) state, and the second transition is observed above 50 mN/m due to the collapse of monolayer into multilayered state [14]. The BAM images (insets) reveal the domain structures during the first transition owing to the coexistence of LC and LE phases [15], but the domains are connected at higher surface pressures and the monolayer becomes immaculate at 35 mN, the target pressure, which represents a cell membrane equivalent surface pressure [16]. In the case of DPPS, π-A isotherm shows single transition state; without LC-LE transition, monolayer is continuously packed until it collapses above 50 mN/m. The BAM analysis also confirms the uniform monolayer state of DPPS at 35 mN/m. Thus, at the target pressure, 35 mN/m, both of phospholipids represent uniformly packed monolayer states. However, DPPS monolayer has a smaller molecular area, thus keeping the more packed state than DPPC.

Penetration of TDP into Model Phospholipid Monolayers

The penetration of the TDP into the model phospholipid monolayer was characterized by the area change of the monolayer, keeping the target pressure at 35 mN/m (Figure 2). Significant increase in the area (~5%) over 10 h was observed for DPPC monolayer, whereas much smaller increase in the first 2 h followed by no further change was observed for DPPS. This tendency is surprising from the following aspects; first, the area increase implies that the direct traverse of the TDP

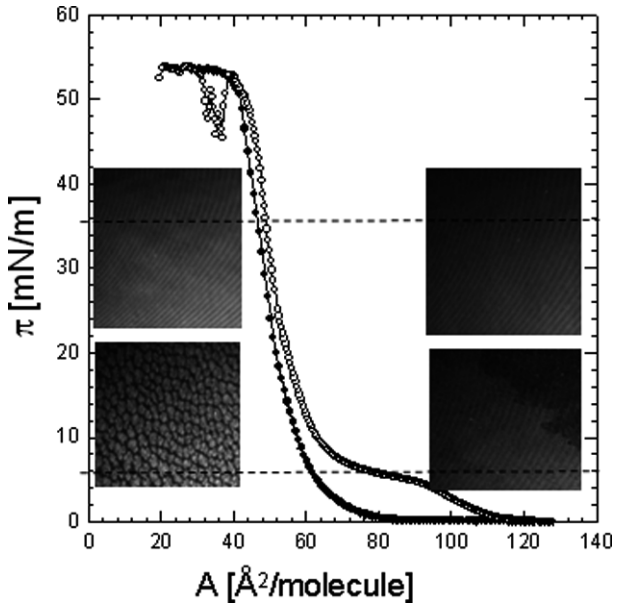

Figure 1 π-A isotherms of DPPC (empty circles) and DPPS (filled circles) on PBS. The left side BAM images for DPPC at 5 (bottom) and 35 mN/m (top), and the right side images for DPPS at the same conditions.

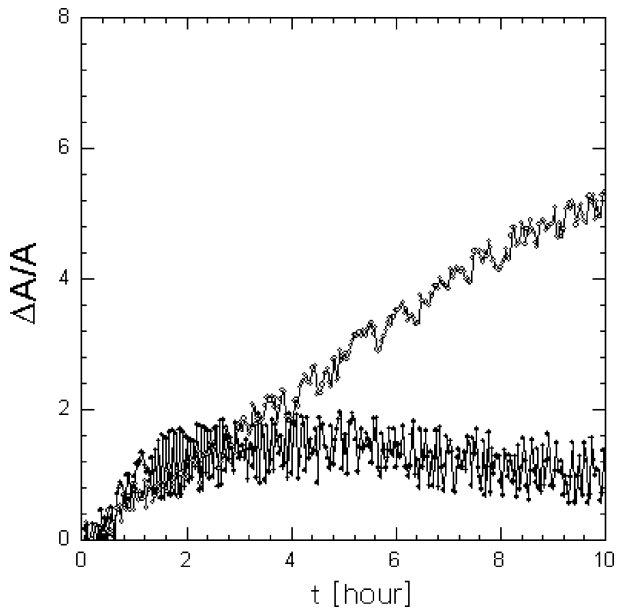

Figure 2 The area changes of DPPS (●) and DPPC (○) monolayers by the penetration of TDP. The subphase concentration of the peptide was 5 μM, and the surface pressure was 35 mN/m.

DOI: 10.1002/psc

across cell membranes via the bare phospholipid bilayer structure might be possible without the support of the cell surface proteoglycans as well as the receptor or the channel on the cell membrane. Second, the more penetration was observed for DPPC than DPPS. The more penetration for DPPS would be expected considering only the charge state: the highly positive charge of the peptide ($z_e = +8$), the net neutral charge of DPPC ($z_e = 0$), and the net-negative charge of DPPS ($z_e = +1$). However, the opposite trend in the area change and the more densely packed state of DPPS than that of DPPC, confirmed by both π-A isotherms (Figure 1) and X-ray reflectivity analysis (Figures 3 and 4) suggest that the highly packed DPPS monolayer at the target pressure may suppress the insertion of peptide into the monolayer, but probably simpler attachment to the monolayer than to the DPPC monolayer owing to the larger driving force from the net-negative charge. In contrast, the DPPC monolayer at the target pressure may have enough space (suggested by more diffusive boundary between headgroup and tail than that of DPPS in Figure 4) to allow the peptide penetration, and the zwitterionic nature of DPPC seems to accommodate the insertion of the positively charged peptide. Nevertheless, the more penetration of the tested CPP onto DPPC also supports the possible existence of the direct penetration pathway of CPP via the bare phospholipid bilayer because DPPC is the most dominant phospholipid in human cells.

Finally, no meaningful surface pressure change was detected by the adsorption of the TDP onto the free surface. Thus, the area increase at the constant surface pressure resulted from the phospholipid-induced penetration of the peptide, not by the surface activity of the peptide itself.

X-ray Reflectivity of Phospholipid Monolayers on PBS

To confirm our hypothesis of the more adsorption but the less penetration of the peptide for DPPS compared to DPPC, we carefully monitored structures of the DPPC and DPPS monolayers before and after the TDP injection by *in situ* X-ray reflectivity.

First, *in situ* X-ray reflectivity measurements before the TDP injection were performed for DPPC and DPPS monolayers, which were compressed to the target pressure of 35 mN/m on PBS (Figures 3(a) and 4(a)). At a glance, the shapes of X-ray reflectivity spectra (closed circles for DPPC and DPPS in Figure 3(a) and 4(a), respectively) of two similar lipids monolayers are very different; the curve from DPPS has a deeper and sharper fringe at a lower q-region, implying that DPPS has a thicker layered structure with narrow interfacial widths at the same target pressure of 35

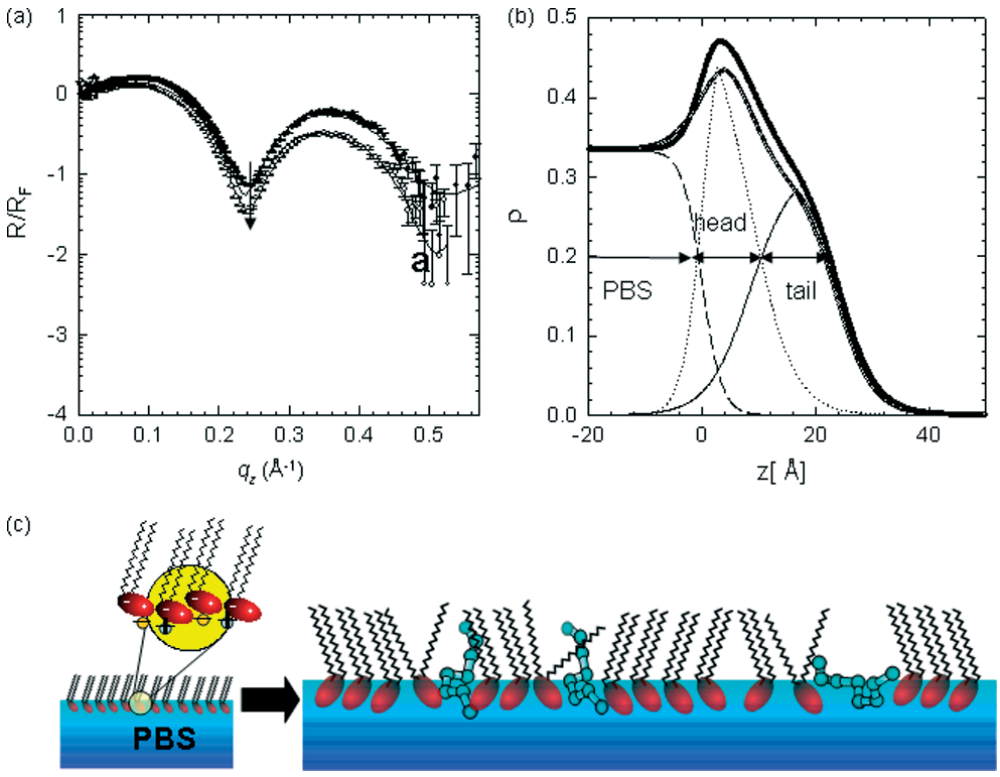

Figure 3 (a) X-ray reflectivity data for pure DPPC (●) and DPPC/TDP (○) films on PBS subphase. (b) The corresponding ρ profiles obtained from the fittings. The total electron density profiles were produced by a *independent* layers (as divided by PBS(dashes), headgroup (dots) and tail (line) profile) which were convoluted to generate continuous model profiles, as described in the text. (c) A schematic representations of the proposed molecular membrane interactions of TDP at DPPC monolayer.

DOI: 10.1002/psc

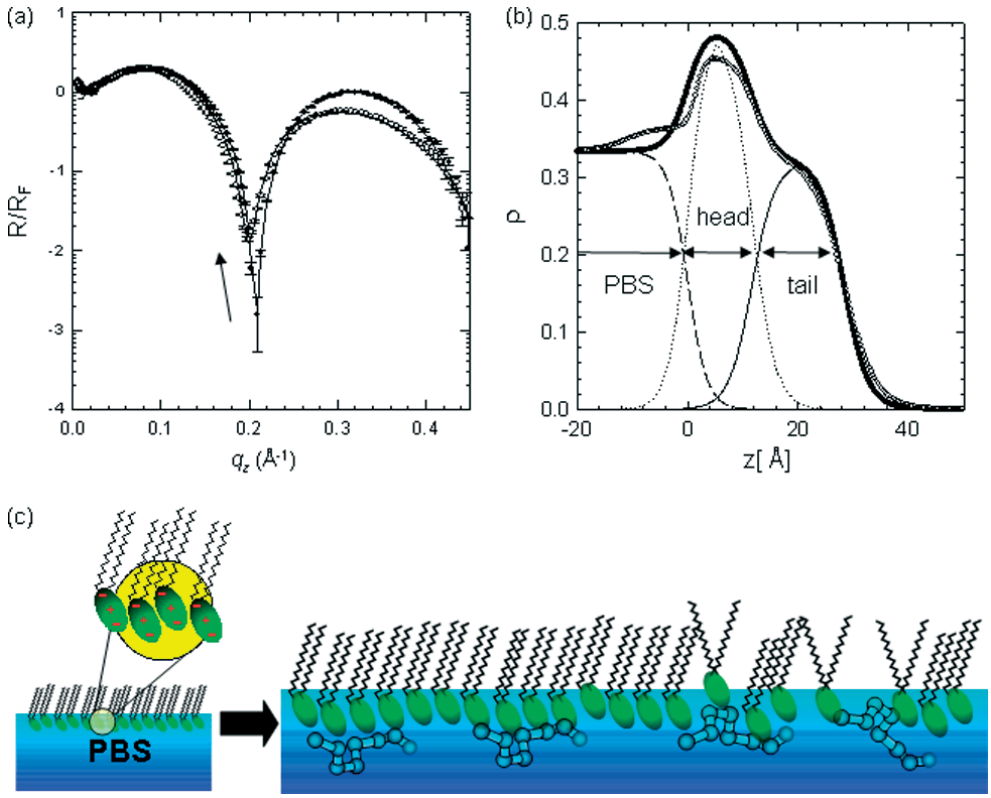

Figure 4 (a) X-ray reflectivity data for pure DPPS (●) and DPPS/TDP (○) films on PBS subphase. (b) The corresponding ρ profiles obtained from the fittings. The total electron density profiles were produced by a *independent* layers (as divided by PBS(dashes), headgroup (dots) and tail (line) profile) which were convoluted to generate continuous model profiles, as described in the text. (c) A schematic representation of the proposed molecular membrane interactions of TDP at DPPS monolayer.

mN/m. To describe the detailed structures, an electron density model perpendicular to the film layer was refined. As previously established by numerous groups [15,17,18], our phospholipid layer model consists of two constant density parts: one corresponding to a polar headgroup region ($\rho_{head} = 0.476$ e$^-$/Å^3), composed of choline, phosphate, and glycerol, and the other corresponding to a hydrophobic hydrocarbon tail region ($\rho_{tail} = 0.321$ e$^-$/Å^3), composed of two hydrocarbon chains. Depending on their electron densities, the indices of refraction of the tail and the headgroup layers differ sufficiently.

To obtain a suitable fitting, we floated three adjustable parameters: the thicknesses of the headgroup and the aliphatic tails, their respective dispersion δ, and the roughnesses at the boundaries (vapor/tail, tail/headgroup, and headgroup/subphase). Note that the number of electrons in the tail molecule was fixed to 242 and the area/molecule (49 Å^2/molecule and 46 Å^2/molecule for DPPC and DPPS, respectively) were fixed to the measured value during the refinement for pure DPPC and DPPS monolayers [19]. Using recursive Parratt formalism, we then varied these values systemically to get the best fitting with reasonable variation of the density, the roughness, and the thickness of each layer. We used the effective-density model [20,21], in contrast to the classical box model; each layer is sliced into very thin pieces (up to 1 Å) with uniform dispersions and sharp interfaces. Figures 3(a) and 4(a) shows that reasonable fits (lines) of DPPC and DPPS monolayer occur over the entire q-range ($\chi^2 < 1$). The refined models of the DPPC and DPPS are shown in Figures 3(b) and 4(b), respectively.

For DPPC, thicknesses of 15.7 ± 0.3 and 8.4 ± 0.3 Å were obtained for a tail region, and a headgroup region, respectively. Taking A of 49 Å^2/molecule from Figure 1 at $\pi = 35$ mN/m, the total electrons participated in the interaction with incident X-ray for the headgroup can be approximated. The electron density (ρ) for the headgroup from the fits was given by $2\pi dA\delta/\lambda^2 r_o$, where d is the thickness of the headgroup. We obtained 0.532 e$^-$/Å^3, and further 219 of the total electrons per molecule were obtained.

Since our aim is to understand the penetration mechanism into the net neutral surface (DPPC) and the net-negative surface (DPPS), it is important to compare the structural differences between DPPC and DPPS monolayers. We similarly analyzed the DPPS monolayer before the TDP adsorption experiments. As mentioned previously, the thicker layered structure is expected for DPPS than DPPC. In fact, 16.6 ± 0.3 Å thick tail layer with an electron density of 0.321 e$^-$/Å^3 (fixed

DOI: 10.1002/psc

value during the refinement) and 11.6 ± 0.3 Å thick headgroup layer with an electron density of 0.496 $e^-/Å^3$ were obtained. The higher packed tail of DPPS results in a tilt angle of 35°, whereas DPPC tail has a tilt angle of 40°. Another discernible point observed for DPPS (Figure 4(b)) is the narrow interfacial widths both at the headgroup/tail interface and the air/tail interface; the fitting results give the interfacial width of 3.8 ± 1.1 and 4.0 ± 1.2 Å, whereas that of DPPC was 6.7 ± 2.0 and 6.0 ± 1.8 Å respectively. On the basis of the fact that DPPS molecules pack more densely as shown in the isotherm, we speculate that the headgroup of DPPS molecule induces tighter molecular packing, which damps the capillary fluctuation effectively [22]. The detailed fitting parameters are listed in Table 1.

X-ray Reflectivity of TDP on Model Phospholipid Monolayers

Figure 3(a) depicts reflectivity before and after addition of 2 μM of TDP for DPPC monolayer. Since the continuous increase in ΔA was observed as circulation continues, the pump was stopped after 10 h and measured. Figure 3(b) shows the corresponding ρ profiles obtained from the best fits. There are a couple of noticeable changes in the reflectivity curve, together with the resulting ρ profile; first, the first minimum (~ 0.24 $Å^{-1}$) is slightly shifted to a lower q-region (see, arrow in the figure), indicating that the total film thickness increases slightly. Further, the overall intensity of the system with the adsorbed TDP is less than that obtained in the absence of TDP, which indicates that the headgroup (which is the highest electron density layer) is disturbed significantly by the penetration of TDP molecules, hence, leading to the lowered electron density of the headgroup region (Figure 3(b)). Interestingly, the additional layer of the adsorbed TDP on the headgroup surface of DPPC is negligible; only an increase in the roughness (the more diffusive boundary) of the headgroup/subphase interface in the density profile is pronounced (Figure 3(b)), in spite of the significant increase in the area of DPPC monolayer by the adsorption and the penetration of the TDP (Figure 4).

In contrast, a substantial density decrease is found at the headgroup/tail region interface (open circles in Figure 3(b)), which might explain how the mean molecular area increased as a function of the adsorption/penetration time; (i) due to the net neutral DPPC headgroup, the positively charged, circulating TDP molecules do not preferentially adsorb and stick to the headgroup surface region. (ii) Since the diffusion flow under the monolayer provide a constant contact of TPD molecules to the DPPC layers, some TPD molecules penetrate through the headgroup region, which are constantly fluctuating owing to their capillary modes, and also are more diffusive and have lower density than that of DPPS (Figure 4). (iii) Consequently, the penetrated TDP molecules entrapped at the headgroup/tail interfacial regions, which induced the substantial density decrease at the headgroup/tail region interface.

It should be noted that that we do not know the exact electron density of the TDP, but e-density of peptides is typically considered in a range of 0.25–0.45 $e^-/Å^3$, depending on the crystal domain structures. However, it is reasonable to assume that the electron density of our TDP is lower than normal proteins, since this peptide mainly consists of highly positive charged, and longer (Lysine and Arginine) amino acids, thus often considered as a linear rod due to its sequential positive charges without 3 dimensional intramolecular structure. Since the electron density of peptides is lower than headgroup (0.471 $e^-/Å^3$), if the peptides are inserted between the headgroup molecules, then the average density must be lowered. Although 5% of expansion due to the insertion of peptides was observed in the isotherm, we could not quantitatively provide the exact amount at the surface, due to the lack of exact electron density of the peptides. Nevertheless X-ray data shows qualitatively that there were some peptides are inserted between headgroups. Further, it is very reasonable that no water molecules exist in the tailgroup, because the tailgroup are composed of two linear aliphatic chains, which are highly hydrophobic. In that case, the expanded region will not be filled efficiently with water molecules, but remained empty [23–25]. Consequently the electron densities of head and tail layer will be reduced by the peptide insertion (Figure 3(c)).

Figure 4(a) shows the reflectivity before and after adsorption and penetration of the TDP for DPPS

Table 1 Fitting parameters obtained from X-ray reflectivity for DPPC and DPPS monolayers on PBS subphase

Sample	A[Å^2][a]	Headgroup region			tail region		
		d [Å]	ρ_m[$e^-/Å^3$]	σ [Å]	d [Å]	ρ_m[$e^-/Å^3$][a]	σ [Å]
DPPC	49	8.4 ± 0.3	0.532	6.7 ± 1.2	15.7 ± 0.3	0.321	6.0 ± 1.8
DPPS	46	11.6 ± 0.3	0.496	3.8 ± 0.8	16.6 ± 0.3	0.321	4.0 ± 1.2

[a] Parameter was fixed during refinement to be the same number of electrons, 242.

DOI: 10.1002/psc

monolayer. The changes in the reflectivity are much clear; essentially, the first minimum shifts to a lower q-region with decreased amplitude. The fitting was performed by including an additional layer on the headgroup layer, keeping the parameters (ρ, d, and σ) for the three layers (tail/headgroup/additional layer) floating during the refinement. Then, a *ca.* 12 Å thick TDP layer underneath the DPPS headgroup region was pronounced clearly in the corresponding density profile (Figure 4(b)). However, in contrast to the DPPC system, the adsorbed TDP molecules do not disturb the tail/headgroup interface much, indicating that most of the adsorbed TDP only remain on the highly negative surface of DPPS headgroup, instead of penetration into the monolayer. This indicates that there are significant amounts of peptides attached on the top of DPPS head group without distracting the monolayer state. Yet, there was some reduction at the headgroup. We speculated that there were some undulation and interference due to the attachment of highly steep rod-like peptide molecules. (Figure 4(c)) No significant reduction of electron density at the tailgroup suggests that the peptides locally remain at the interface between headgroup and liquid interface, and only minimal insertion occurred.

Combining the much less increase in ΔA and the density profile results from the reflectivity, it can be concluded that the preferential binding to the negatively charged headgroup does not result in an efficient penetration into the monolayer, which would lead to an increase in the mean molecular area of DPPS.

CONCLUSIONS

At 35 mN/m, a cell-membrane equivalent surface pressure, DPPS monolayer is more packed with a sharp interface boundary while DPPC monolayer is less packed with a more diffusive headgroup/subphase boundary, although both phospholipids formed a homogeneous monolayer state. The penetration of the peptide into the phospholipid monolayer is evident from the increase in the surface area at the target pressure, which support the existence of a direct penetration mechanism of the peptide across the pure phospholipid bilayer membrane. Contrary to the simple charge interaction, the more significant area increase was monitored from DPPC monolayer. X-ray reflectivity measurements as well as the molecular area from π-A isotherms suggest that the packing density of DPPS at the target pressure is too high to allow the effective penetration of the peptide into the monolayer; the peptides mainly lead to the simple adsorption on the monolayer instead of penetration into it. We also infer that the positive peptide can be entrapped at the negative electrostatic well of DPPS headgroup layer, thus no further penetration is hindered. Thus, the more penetration with the less adsorption of the peptide is induced by DPPC monolayer than DPPS monolayer.

Acknowledgements

This work was supported by a grant (05K1501-01311) from 'Center for Nanostructured Materials Technology' under '21st Century Frontier R and D Program', BAERI and KRF (D00058), Korea.

REFERENCES

1. Zorko M, Langel U. Cell-penetrating peptides: mechanism and kinetics of cargo delivery. *Adv. Drug Deliv. Rev.* 2005; **57**: 529–545.
2. Albarran B, To R, Stayton PS. A TAT-streptavidin fusion protein directs uptake of biotinylated cargo into mammalian cells. *Protein Eng. Des. Sel.* 2005; **18**: 147–152.
3. Brooks H, Lebleu B, Vives E. Tat peptide-mediated cellular delivery: back to basics. *Adv. Drug Deliv. Rev.* 2005; **57**: 559–577.
4. Lindgren M, Hallbrink M, Prochiantz A, Langel U. Cell-penetrating peptides. *Trends Pharmacol. Sci.* 2000; **21**: 99–103.
5. Frankel AD, Pabo CO. Cellular uptake of the tat protein from human immunodeficiency virus. *Cell* 1988; **55**: 1189–1193.
6. Green M, Loewenstein PM. Autonomous functional domains of chemically synthesized human immunodeficiency virus tat trans-activator protein. *Cell* 1988; **55**: 1179–1188.
7. Vives E, Brodin P, Lebleu B. A truncated HIV-1 Tat protein basic domain rapidly translocates through the plasma membrane and accumulates in the cell nucleus. *J. Biol. Chem.* 1997; **272**: 16010–16017.
8. Derossi D, Joliot AH, Chassaing G, Prochiantz A. The third helix of Antennapedia homeodomain translocates through biological membranes. *J. Biol. Chem.* 1994; **269**: 10444–10450.
9. Ziegler A, Blatter XL, Seelig A, Seelig J. Protein transduction domains of HIV-1 and SIV TAT interact with charged lipid vesicles: binding mechanism and thermodynamic analysis. *Biochemistry* 2003; **42**: 9185–9194.
10. Tyagi M, Rusnati M, Presta M, Giacca M. Internalization of HIV-1 Tat requires cell surface heparan sulfate proteoglycans. *J. Biol. Chem.* 2001; **276**: 3254–3261.
11. Tanford C. *The Hydrophobic Effect: Formation of Micelles and Biological Membranes*. Wiley: New York, 1973; 93.
12. Russell TP. X-ray and neutron reflectivity for the investigation of polymers. *Mater. Sci. Rep.* 1990; **5**: 171–271.
13. Miller CE, Majewski J, Gog T, Kuhl TL. Characterization of biological thin films at the solid-liquid interface by X-ray reflectivity. *Phys. Rev. Lett.* 2005; **94**: 238104.
14. Georgallas A, Pink DA. A new theory of the liquid condensed-liquid expanded phase transition in lipid monolayers. *Can. J. Phys.* 1982; **60**: 1678–1681.
15. McConlogue CW, Vanderlick TK. A close look at domain formation in DPPC monolayers. *Langmuir* 1997; **13**: 7158–7164.
16. Seelig A. Local anesthetics and pressure, a comparison of dibucarine binding to lipid monolayers and bilayers. *Biochim. Biophys. Acta* 1987; **899**: 196–204.
17. Kuhl TL, Majewski J, Howes PB, Kjaer K, von Nahmen A, Lee KYC, Ocko B, Israelachvili JN, Smith GS. Packing stress relaxation in polymer–lipid monolayers at the air–water interface: an X-ray grazing incidence diffraction and reflectivity study. *J. Am. Chem. Soc.* 1999; **121**: 7682–7688.
18. Kim K, Shin K, Kim H, Kim C, Byun Y. In situ photopolymerization of a polmerizable poly(ethylene glycol)-covered phospholipid monolayer on a methacryloyl-terminated substrate. *Langmuir* 2004; **20**: 5396–5402.

19. Wu G, Majewski J, Ege C, Kjaer K, Weygand MJ, Lee KY. Interaction between lipid monolayers and poloxamer 188: an X-ray reflectivity and diffraction study. *Biophys. J.* 2005; **89**: 3159–3173.
20. Tolan M. *X-ray Scattering from Soft-matter Thin Films*. Springer-Verlag: Berlin, 1999.
21. Kim K, Byun Y, Kim C, Kim TC, Noh DY, Shin K. Combined study of X-ray reflectivity and atomic force microscopy on a surface-grafted phospholipid monolayer on a solid. *J. Colloid Interface Sci.* 2005; **284**: 107–113.
22. Daillant J. X-ray scattering at liquid surfaces and interfaces. *Curr. Sci.* 2000; **78**: 1496–1506.
23. Neville F, Cahuzac M, Konovalov O, Ishitsuka Y, Lee KYC, Kuzmenko I, Kale GM, Gidalevitz D. Lipid headgroup discrimination by antimicrobial peptide LL-37: insight into mechanism of action. *Biophys. J.* 2006; **90**: 1275–1287.
24. Gidalevitz D, Huang Z, Rice SA. Protein folding at the air-water interface studied with x-ray reflectivity. *Proc. Natl. Acad. Sci.* 1999; **96**: 2608–2611.
25. Baneyx G, Vogel V. Self-assembly of fibronectin into fibrillar networks underneath dipalmitoyl phosphatidylcholine monolayers: role of lipid matrix and tensile forces. *Proc. Natl. Acad. Sci.* 1999; **96**: 12518–12523.

DOI: 10.1002/psc